Dynamical Mass Estimates of Large#Scale Filaments in Redshift Surveys

Citation

Permanent link

Terms of Use

Share Your Story

DYNAMICAL MASS ESTIMATES OF LARGE-SCALE FILAMENTS IN REDSHIFT SURVEYS

Daniel J. Eisenstein[1] and Abraham Loeb[2]

Astronomy Department, Harvard University, 60 Garden Street, Cambridge, MA 02138

AND

Edwin L. Turner[3]

Princeton University Observatory, Princeton University, Peyton Hall, Princeton, NJ 08544

ABSTRACT

We propose a new method to measure the mass of large-scale filaments in galaxy redshift surveys. The method is based on the fact that the mass per unit length of isothermal filaments depends only on their transverse velocity dispersion. Filaments that lie perpendicular to the line of sight may therefore have their mass per unit length measured from their thickness in redshift space. We present preliminary tests of the method and find that it predicts the mass per unit length of filaments in an N-body simulation to an accuracy of $\sim 35\%$. Applying the method to a select region of the Perseus-Pisces supercluster yields a mass-to-light ratio of $M/L_B \approx 450\ h$ in solar units to within a factor of 2. The method measures the mass-to-light ratio on mass scales up to 10 times that of clusters of galaxies and could thereby yield new information on the behavior of the dark matter on large scales.

Subject headings: dark matter — galaxies: clusters: individual (Perseus-Pisces) — galaxies: distances and redshifts — galaxies: fundamental parameters — large-scale structure of universe

1. INTRODUCTION

It has long been known that galaxies are not spread evenly throughout the universe but instead are organized into larger structures stretching out to scales ~ 100 Mpc (Einasto, Joeveer, & Saar 1980; Peebles 1993, § 3). Large redshift surveys (see Strauss & Willick 1995 for a review) mapped this structure in three dimensions and showed that in addition to the conspicuous clusters of galaxies, there are also extended one-dimensional filaments (Haynes & Giovanelli 1986) and two-dimensional sheets (de Lapparent, Geller, & Huchra 1986; Geller & Huchra 1989; Shectman et al. 1996). The observed geometries can be explained by gravitational instability theories of structure formation, both through analytical approximations (Zel'dovich 1970; Bond, Kofman, & Pogosyan 1995; Eisenstein & Loeb 1995; Bond & Myers 1996), and numerical simulations (e.g., Bertschinger & Gelb 1991; Park et al. 1994; Cen & Ostriker 1994).

The filaments and sheets that are observed in galaxy surveys represent the most massive nonlinear structures in the local universe. While these structures are painted by the light emitted from galaxies, their actual mass distribution is unknown. Determining the mass is particularly difficult because these systems are still evolving along one or two axes. Less massive systems such as galaxies and galaxy clusters have generally virialized by now, and their dynamics unambiguously imply substantial amounts of dark matter (Rubin 1983; Trimble 1987; David, Jones, & Forman 1995). While the dynamical estimates of the mass-to-light ratio of virialized systems argue for an open universe (e.g., Bahcall, Lubin, & Dorman 1995), it is unknown whether more mass, sufficient to close the universe, remains undetected outside

virialized objects. Methods to measure the mass on larger scales include peculiar velocity studies (see Strauss & Willick 1995, and references within), analyses of superclusters (Postman, Geller, & Huchra 1988; Raychaudhury et al. 1991; Baffa et al. 1993), and the inferences based on cosmic microwave background anisotropies (Jungman et al. 1996). In addition to the implications for the value of the cosmic density parameter Ω, such measurements provide insight into the clustering properties of the dark matter and the degree of biasing in galaxy formation.

In this paper, we present a novel method for measuring the mass of large-scale filaments that is based purely on the information available in redshift surveys. The method relies on the observation that while spherical and planar geometries require both a characteristic velocity and a characteristic length to estimate mass, a cylindrical system requires only a velocity dispersion to estimate its mass per unit length. On dimensional grounds, the mass per unit length times Newton's constant must be proportional to the transverse velocity dispersion squared of the filament. For filaments oriented across the sky, i.e., perpendicular to the line of sight, the velocity dispersion is measured as the thickness of the structure in redshift space. Since the length of such a filament is readily apparent from its angular extent, the method allows the determination of the mass-to-light ratio on scales beyond that of clusters, despite the fact that the objects of interest are neither fully virialized nor in the linear perturbative regime.

In § 2, we present an exact solution to the Jeans equation for the case of an isothermal, axisymmetric, steady state filament. This derivation extends the well-known hydrodynamic solutions for isothermal gases (Stodółkiewicz 1963; Ostriker 1964) to collisionless systems. With this solution at hand, we present tests of the method in § 3, focusing primarily on filaments selected in real space from an N-body simulation. While not definitive, the results are encouraging, suggesting that accuracy $\sim 35\%$ in mass is attainable. In § 4 we conclude with a discussion of the ingredients of

[1] Also at Physics Department, Harvard University. Present address: Institute for Advanced Study, Princeton, NJ 08540; eisenste@sns.ias.edu.

[2] aloeb@cfa.harvard.edu.

[3] elt@astro.princeton.edu.

more elaborate scheme to calibrate the method and demonstrate its robustness. We also apply the method as it stands to the Perseus-Pisces supercluster and estimate a B-band mass-to-light ratio of $450\,h$ in solar units.

2. ANALYTIC RESULTS

Let us first derive an exact analytical solution to the Jeans equations for the case of an axisymmetric, isothermal, steady state filament that is translationally invariant along its symmetry axis. Solutions for isothermal gaseous filaments in hydrostatic equilibrium (Stolółkiewicz 1963; Ostriker 1964) lead the way. We begin with the Jeans equations in cylindrical coordinates (R, θ, z) and assume axial symmetry and no bulk velocity in the radial (transverse) direction. The radial Jeans equation is

$$\frac{\partial(v\langle v_R^2\rangle)}{\partial R} + v\frac{\langle v_R^2\rangle - \langle v_\theta^2\rangle}{R} = -v\frac{\partial\Phi}{\partial R}, \tag{1}$$

where v is the number density of particles, $\langle v_R^2\rangle$ and $\langle v_\theta^2\rangle$ are the ensemble averages of the squares of the radial velocities and tangential velocities, respectively, and Φ is the gravitational potential. All of these quantities are functions of R only. Gravity is determined from the Poisson equation

$$\frac{1}{R}\frac{\partial}{\partial R}\left(R\frac{\partial\Phi}{\partial R}\right) = 4\pi G\rho, \tag{2}$$

where G is Newton's constant and $\rho \propto v$ is the mass density.

We now assume that $\langle v_R^2\rangle$ and $\langle v_\theta^2\rangle$ are related by a constant $\beta = 1 - \langle v_\theta^2\rangle/\langle v_R^2\rangle$. As in the case of analysis of spherical systems (Binney & Tremaine 1987), $\beta = 1$ indicates purely radial orbits, $\beta = 0$ indicates isotropic orbits, and $\beta = -\infty$ indicates purely tangential orbits. The introduction of β reduces equation (1) to

$$\frac{1}{v}\frac{\partial(v\langle v_R^2\rangle)}{\partial R} + \beta\frac{\langle v_R^2\rangle}{R} = -\frac{\partial\Phi}{\partial R}. \tag{3}$$

We now assume that the filament is isothermal, so that $\langle v_R^2\rangle(R) = \sigma^2$. This yields

$$\sigma^2\left(\frac{\partial\log\rho}{\partial\log R} + \beta\right) = -R\frac{\partial\Phi}{\partial R}. \tag{4}$$

Note that this equation is scale-free in radius.

We next introduce the mass per unit length enclosed within a radius R

$$\mu(R) = 2\pi\int_0^R \tilde{R}\rho(\tilde{R})d\tilde{R}. \tag{5}$$

Inserting equation (2) yields

$$\mu = \frac{1}{2G}R\frac{\partial\Phi}{\partial R}, \tag{6}$$

which in turn may be used in equation (4) to yield

$$\frac{\sigma^2}{2G}\left(\frac{R}{\rho}\rho' + \beta\right) = -\mu, \tag{7}$$

where primes indicate differentiation with respect to R. From equation (5), we find $\mu' = 2\pi R\rho$, which we use to eliminate ρ in favor of μ. The resulting equation is

$$R\mu'' + (\beta - 1)\mu' + \frac{2G}{\sigma^2}\mu\mu' = 0. \tag{8}$$

Since $R\mu'' = d(R\mu' - \mu)/dR$, we may integrate equation (8) to get

$$R\mu' + (\beta - 2)\mu + \frac{G\mu^2}{\sigma^2} = 0; \tag{9}$$

since $\mu(0) = 0$, the constant of integration is zero. We may then integrate again and solve for μ to find

$$\mu(R) = (2 - \beta)\frac{\sigma^2}{G}\frac{R^{2-\beta}}{R^{2-\beta} + R_0^{2-\beta}}, \tag{10}$$

where R_0 is an arbitrary scale factor. Therefore, the mass per unit length at radii much larger than R_0 is finite and approaches $(2 - \beta)\sigma^2/G$.

We may differentiate $\mu(R)$ to find the density profile

$$\rho = \frac{(2 - \beta)^2\sigma^2}{2\pi GR_0^2}\frac{x^{-\beta}}{(x^{2-\beta} + 1)^2}, \tag{11}$$

where $x = R/R_0$. Hence, $\rho \propto x^{-\beta}$ at small radii and $\rho \propto x^{\beta-4}$ at large radii. The small radii behavior is unphysical for $\beta < 0$ (i.e., predominantly tangential orbits).

Finally, we consider what velocity dispersion is measured along a line of sight perpendicular to the axis of symmetry. Assuming that the filament is axisymmetrically sampled, we find that the measured one-dimensional velocity dispersion orthogonal to the symmetry axis is

$$\sigma_\perp^2 = \frac{\langle v_R^2\rangle + \langle v_\theta^2\rangle}{2}. \tag{12}$$

Inserting our assumptions concerning the ratio of the velocity dispersions and isothermality, this becomes $\sigma_\perp^2 = \sigma^2(1 - \beta/2)$. Hence, we find that the total mass per unit length of the filament (defined for $R \gg R_0$) is

$$\mu = \frac{2\sigma_\perp^2}{G} = 7.4 \times 10^{13}\,M_\odot\,\text{Mpc}^{-1}\left(\frac{\sigma_\perp}{400\,\text{km s}^{-1}}\right)^2. \tag{13}$$

The dependence on β has canceled out. Indeed, the assumptions of isothermality and constancy of β may prove unimportant, since Milgrom (1997) shows that they can be relaxed in the limit of axisymmetry.

3. NUMERICAL TESTS ON REAL-SPACE FILAMENTS

Based on the discussion in § 2, we propose to use the observed velocity dispersion as a means of calibrating the mass per unit length of a filament of galaxies in a galaxy redshift survey. Here one would study filaments that are aligned perpendicular to the line of sight; the velocity dispersion then manifests itself as the thickness of the filament in redshift space. By measuring the mass per unit length of such structures, one can find their mass-to-light ratios and thereby probe the properties of dark matter on large scales. However, the analytic results of the last section were derived under a particular set of idealized assumptions. The filaments of galaxies in a redshift survey do not satisfy all these assumptions, and therefore the validity of equation (13) needs to be checked against one-dimensional structures in numerical simulations.

The most drastic violation of the assumptions underlying § 2 is due to omnipresent substructure, often in the form of fragmentation along the filament (Chandrasekhar & Fermi 1953; Stodółkiewicz 1963; Larson 1985). What one takes as a filament actually more resembles a chain of differently

sized beads. Substructure tends to cause an overestimation of the mass per unit length, essentially because vacant areas along the filament are credited with having mass when in fact they are empty. For example, if a "filament" were actually a string of N widely spaced isothermal spheres of velocity dispersion σ and radius R, then the true mass would be $2\,\sigma^2 NR/G$. But the filamentary mass estimate is $2\,\sigma^2 L/G$, where L is the length of the filament, an overestimate by a factor of L/NR, or twice the filling fraction of the isothermal spheres.

Another key difference is that the filaments are not isolated but instead are subject to continuing infall and perturbations from neighboring mass concentrations. The transverse crossing time across the filament is much shorter than the Hubble time, and so the filament core may virialize. However, the infalling material violates the assumption of steady state radial equilibrium; moreover, due to the associated redshift distortion (Sargent & Turner 1977; Kaiser 1987), it makes the filament look thinner (i.e., have a lower σ) than it actually is. Self-similar infall solutions for filamentary geometries have been found in both collisionless and collisional systems (Fillmore & Goldreich 1984; Inutsuka & Miyama 1992; Gehman et al. 1996), and so one could imagine deriving the equivalent of equation (13) for these collapse solutions. However, because the mass inside a particular radius diverges as the radius increases in these infall models, it is unclear how to define the total mass per unit length of a redshift space filament. Moreover, if the background cosmology is not scale-free, then the self-similar solution loses its justification. All solutions, infalling or isolated, will produce $\mu \propto \sigma^2/G$ by dimensional analysis, and so we see no compelling reason to disfavor the coefficient of 2 found in the isolated case relative to other approximations. Instead we calibrate this coefficient using N-body simulations.

Finally, real filaments are not infinitely long, exactly straight, or perfectly isothermal and axisymmetric. The effects of finite length or curvature may be characterized by a length scale, either the length or radius of curvature, which are then compared to the characteristic width of the filament. In either case, the fact that this length scale is larger than the length scale we expect to be associated with fragmentation suggests that these effects will be smaller than the deviations caused by fragmentation. The isothermal assumption has worked well in spherical systems but remains to be tested in this case. Deviations from axisymmetry will cause variations in the inferred mass per unit length as a function of viewing angle; we will estimate the magnitude of the variations later in this section.

We see two methods for testing the applicability of equation (13). First, we may select filamentary structures in real space from N-body simulations. This procedure utilizes information that is not available in redshift surveys, but it does allow us to test whether this dynamical mass estimation formula holds for systems that stretch the idealizations under which it was derived. In particular, we may investigate the role of substructure within the filament. Second, we may select the filaments in redshift space from mock surveys culled from simulations. This allows one to examine the effects of contamination from foreground and background galaxies, to experiment with selection effects, and to calibrate the method in a robust way. We focus on the first of these methods in this paper, although we will devote some discussion to the second.

For our testing, we use an open CDM particle-mesh (PM) N-body simulation provided by C. Park and J. R. Gott (Park et al. 1994). The simulation has $240^3 = 13.8 \times 10^6$ particles and a 480^3 mesh; the background cosmology is $\Omega = 0.4$, $\Lambda = 0$, and $H_0 = 50$ km s^{-1} Mpc^{-1}. The simulation volume is $576\,h^{-3}$ Mpc^3, yielding a particle mass of $1.5 \times 10^{12}\,h^{-1}\,M_\odot$, where $h = H_0/(100$ km s^{-1} Mpc$^{-1}) = 0.5$. We use only the $z = 0$ output. Typical filaments have masses around $3 \times 10^{15}\,h^{-1}\,M_\odot$ and lengths of order $50\,h^{-1}$ Mpc. They are generally a few, but rarely more than 10, mesh cells thick; the mass per unit length is such that there are on average 30 particles per lengthwise mesh spacing.

3.1. Real-Space Selected Filaments

For our tests on real-space selected filaments, we select filaments by eye from cross-sectional slices. We look for candidates that appear to be roughly linear arrangements of particles. By looking at orthogonal cross sections, we verify that the object is indeed a filament rather than a chance superposition. We then choose two endpoints of a line segment to describe the center of the filament; the filament is defined as a cylindrical volume of a particular radius around this line segment.

The choice of the filament's boundary radius is not unique. While one might expect the steady state assumption in the idealized derivation to apply only to the densest regions, where the particles have executed several radial crossings of the filament, this is not the region that will be picked out in a redshift survey. Redshift-space distortions will cause objects infalling onto the filament to be confused with those in the collapsed region. For example, a particle at turnaround has zero radial velocity relative to the center of the filament and therefore has the same redshift. To pick a radius characteristic of this infall region, we select the radius at which the average density within that cylinder is 5.7 times the background density. This is the value for the density at turnaround of a collapsing homogeneous filament in an $\Omega = 0.4$ universe (for reference, the value would be 3.5 for $\Omega = 1$ and 8.9 for $\Omega = 0.2$). As we show later, our density definition indeed selects the turnaround radius of actual filaments in an N-body simulation. We denote this radius by R_{ta}.

Small filaments may be underresolved by the PM code; we therefore require that within the radius R_{ta} the filament contains at least 500 particles and has an average linear density exceeding 12.5 particles per lengthwise mesh spacing. This leaves us with 23 filaments; the largest ones are 6 times more massive than the minimum mass requirement.

We next consider "observing" these particles from a direction orthogonal to the filament axis. Because we are interested in the velocity dispersion of the particles rather than in their bulk motions, we do not want variations in bulk velocity along the filament to be included in its redshift "thickness." In particular, a filament that is orthogonal to the viewer's line of sight in real space may be slightly tilted or warped in redshift space, and we do not want such variations to enter the velocity dispersion. Therefore, we break the filament lengthwise into 20 equal pieces and remove the mean velocity in each piece from the velocity of the particles in the section before calculating the velocity dispersion.

Taking the axis of the filament to be the z axis, we consider observing the filament from directions in the x-y

plane. Different viewing angles yield different estimates for the line-of-sight velocity dispersion; however, these varying answers are in fact only different combinations of σ_{xx}, σ_{yy}, and σ_{xy}, where for example

$$\sigma_{xy}^2 = \frac{1}{N} \sum_{\text{particles}} v_x' v_y' \, , \qquad (14)$$

where v_i' is the ith component of the velocity of a particle after the mean velocity of its section of the filament has been subtracted, and N is the total number of particles. Forming the matrix

$$\Sigma = \begin{pmatrix} \sigma_{xx}^2 & \sigma_{xy}^2 \\ \sigma_{xy}^2 & \sigma_{yy}^2 \end{pmatrix} \, , \qquad (15)$$

and considering an observer at infinite distance from direction $\hat{n}$ in the x-y plane, the velocity dispersion in that direction is simply $(\hat{n}^T \Sigma \hat{n})^{1/2}$. Therefore, by diagonalizing Σ, we find the largest and smallest possible measurements of $\sigma_\perp^2$ that can result from differing viewing angles. The figures show these two extremal estimates for the mass per unit length; the ratio between them is usually $\lesssim 2$.

In Figure 1, we show the comparison for the 23 filaments between the true mass per unit length within R_{ta}, $\mu_{\text{true}}(R_{ta})$, and the two extreme estimates $\mu_{\text{est}}(R_{ta})$ based on the measurement of $\sigma_\perp^2$. Figure 2 shows the ratio $\tilde{\mu} = \mu_{\text{est}}(R_{ta})/\mu_{\text{true}}(R_{ta})$ versus $\mu_{\text{true}}(R_{ta})$. Here we see that the estimate is in almost all cases within a factor of 2 of the true value, and with this sample there is no obvious correlation between μ_{true} and $\tilde{\mu}$. Taking all viewing angles as equally likely, this ensemble of 23 filaments yields a distribution of $\tilde{\mu}$ with a mean of 1.17 and a 1 σ error of 0.39. In other words, the estimate of μ from equation (13) is biased 17% high; with this removed, one finds a mass estimate with 33% accuracy.
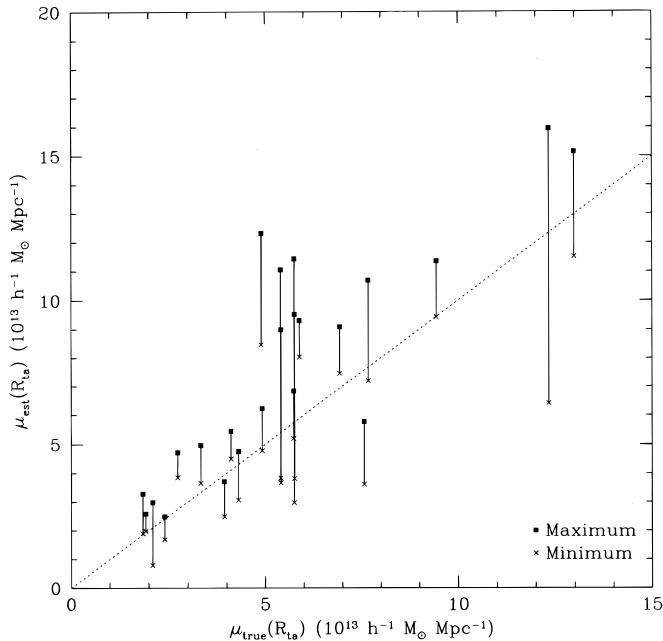

FIG. 1.—Mass per unit length as estimated from the velocity dispersion of the particles within radius R_{ta} plotted against the actual mass per unit length within radius R_{ta}. The plot shows the full range of possible estimates if one considers all viewing angles in the plane perpendicular to the axis of the filament.
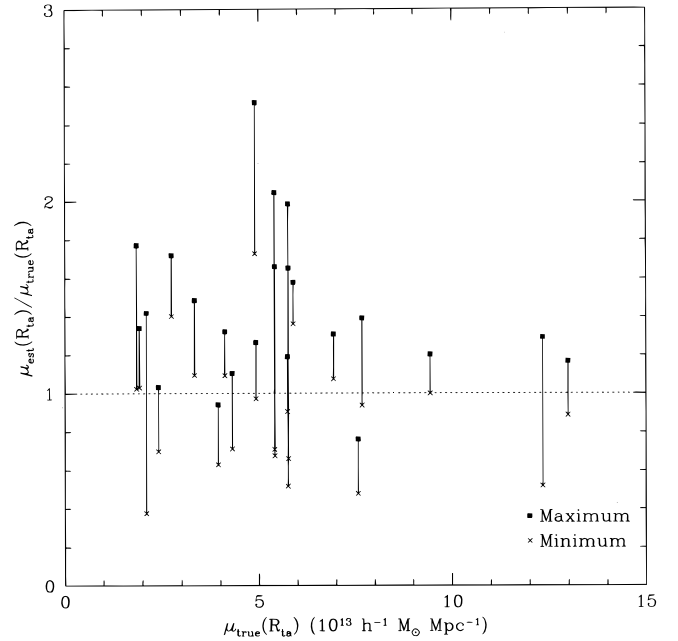

FIG. 2.—Same as Fig. 1, but shown is the ratio of the estimated mass per unit length μ to the true value vs. the true μ.

Because the filament is laid out across the sky, the substructure and clumpiness along its length are observable. We would expect that applying our method to filaments with more substructure would produce larger estimates of the mass per unit length, essentially because one is crediting the lower density regions with the velocity dispersion of the higher density regions. We consider several different statistics to measure the degree of substructure. First, we break the filament into 20 lengthwise pieces, count the number of particles in each piece, and take the ratio of the standard deviations of these 20 numbers to their mean as one statistic. Next, we bin the particles into 128 lengthwise bins and perform the cosine transform (Press et al. 1992) on the vector of occupation numbers. We then add up the power in the 10, 15, or 20 lowest modes (normalizing away the dependence on the number of bins and the number of particles) and use these as measures of substructure.

In Figure 3, we plot the power in the 10 lowest cosine modes, S_{10}, versus the ratio $\tilde{\mu}$ of the estimated to true mass per unit length. There is a fair correlation ($r = 0.53$) in the expected direction. The other substructure statistics produce very similar results. In applying this program to real survey data, one might plan to reject filaments with large measures of substructure. If we remove the six filaments with S_{10} larger than 0.9, then the remaining 17 filaments produce a distribution of $\tilde{\mu}$ with mean 1.07 and error 0.31 (29%).

Next, we examine the dependence of the velocities on radius. In Figure 4, we show the azimuthally averaged profiles for the mean radial velocity $\langle v_R \rangle(R)$ and radial velocity dispersion $\sigma_R(R)$ for several particular filaments. We also show the average value of $\sigma_\perp$ that can be measured from the particles within the given radius. The profiles $\langle v_R \rangle(R)$ tend to cross zero near R_{ta}, showing that R_{ta} is indeed a reasonable choice for the turnaround radius. The profiles of $\sigma_R(R)$ show deviations from isothermality at large radii; because $\sigma_\perp$ is a cumulative statistic, these deviations do not affect the measured velocity dispersion much. For the full sample of
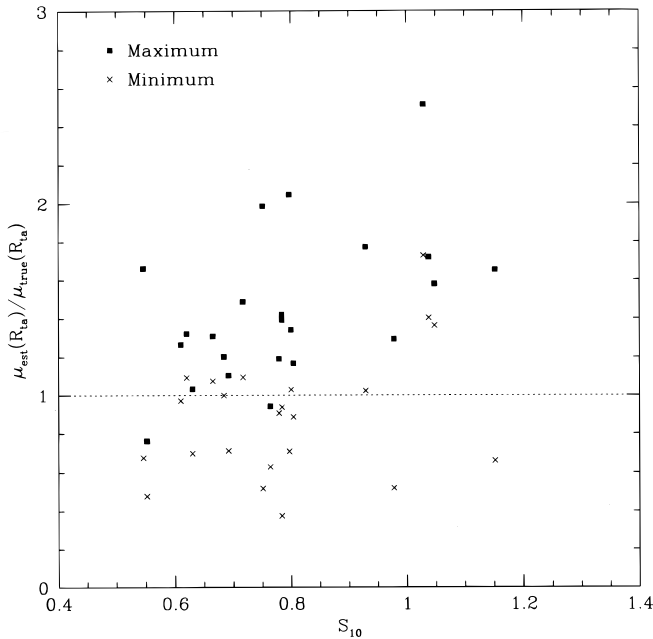
FIG. 3.—Ratio of the estimated mass per unit length to the true value vs. a measure of substructure within the filament. The statistic S_{10} is the sum of the power in the lowest 10 modes of the cosine transform; larger values indicate more substructure.

23 filaments, the ratio of $\sigma_R(R_{ta})$ to the value of σ_R for all particles within $R_{ta}/2$ has a mean of 0.80 with error 0.247; that is, the velocity dispersion at R_{ta} is roughly 80% of the value in the central regions. Finally, we find that the average value of the velocity anisotropy parameter β is zero (isotropic) at all radii but with significant scatter (1 $\sigma \sim$ 0.3).

In summary, the method of predicting the mass per unit length of a filament from its observed velocity dispersion does reasonably well in real-space tests of an N-body simulation. Because the procedures of this section did not confront the confusion caused by redshift distortions and foreground/background galaxies or the missteps possible in picking one-dimensional structures from a discrete set of points, we do not consider these tests definitive. Nevertheless, it is encouraging that the method performs to an accuracy of $\lesssim 40\%$ despite significant substructure, departures from axisymmetry and isothermality, and some inclusion of infall.

3.2. *A First Step into Redshift Space*

We next apply the method to a simulated redshift survey. Using the same PM simulation as above, we select a mock survey by giving each particle an equal chance to be a galaxy, assuming a Schechter luminosity function, and applying an apparent magnitude cutoff. The survey geometry is chosen to be a slice 1°.5 thick and 90° wide, and the depth is similar to that of the Las Campanas Redshift Survey (LCRS) (Shectman et al. 1996; Lin et al. 1996; Landy et al. 1996). We use the adjacent slices to verify that our filaments are not cuts through sheets. The real-space plot of the particles in shown in Figure 5; the plot of the mock redshift survey drawn from the slice is shown in Figure 6.

Within the slice, two large transverse filaments are apparent. We flag the "galaxies" that appear as part of the filament. The galaxies selected this way are highlighted in
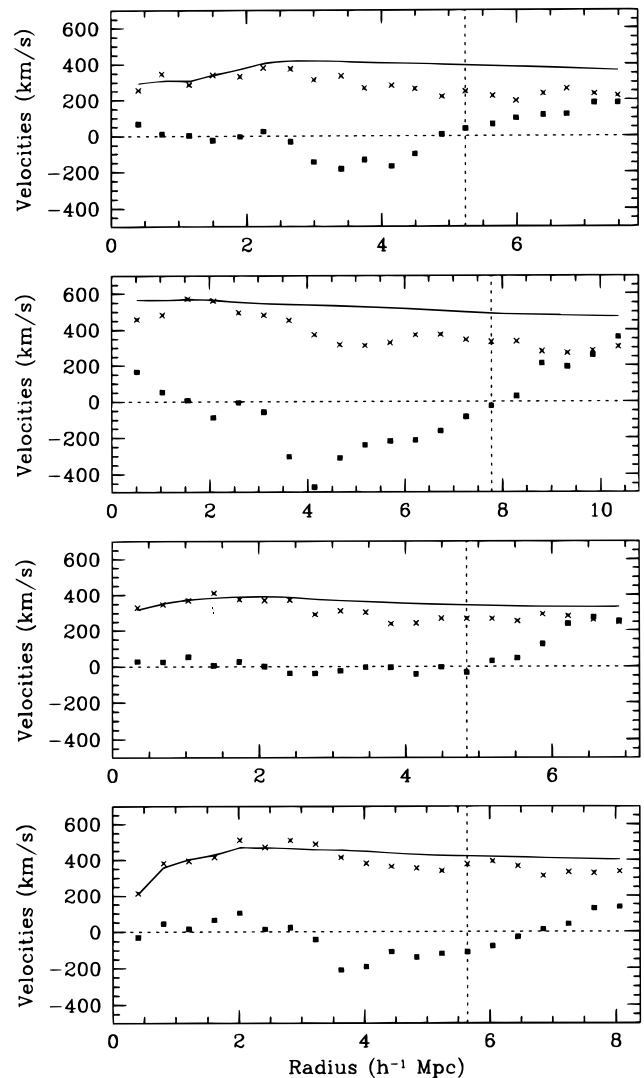

FIG. 4.—Velocity profiles of four filaments from the sample. For each radial bin, we show the mean radial velocity (*squares*) and the radial velocity dispersion (*crosses*). Also shown is the average transverse velocity dispersion of all particles within the stated radius (*solid line*). The vertical dashed lines mark R_{ta} in each case. The third and fourth panels show the regions marked in Fig. 5 as filaments A and B, respectively.

Figure 6. Within a set of galaxies, we fit a straight line in redshift space and measure the residual velocity spread around the line to find the velocity dispersion $\sigma_\perp$. Because the filaments have rather little extent in redshift, we neglect variations in the selection function across the set and give each galaxy equal weight in the velocity dispersion. We also neglect the small angle between the observed line of sight and the direction perpendicular to the axis of the filament. More refined analyses could include these effects. Our measurement of $\sigma_\perp$ then gives the mass per unit length, which we multiply by the length (angular length times distance) to get the total mass.

In order to compare the mass estimate to the true answer, we find it most convenient to use our knowledge of the luminosity function in order to convert our result to an estimate of Ω. Taking the filament to be at a single distance, we find Ω as the ratio between the estimated mass per observed galaxy and the critical mass per observable galaxy, which is the critical density divided by the number density of galaxies observable at that distance given the
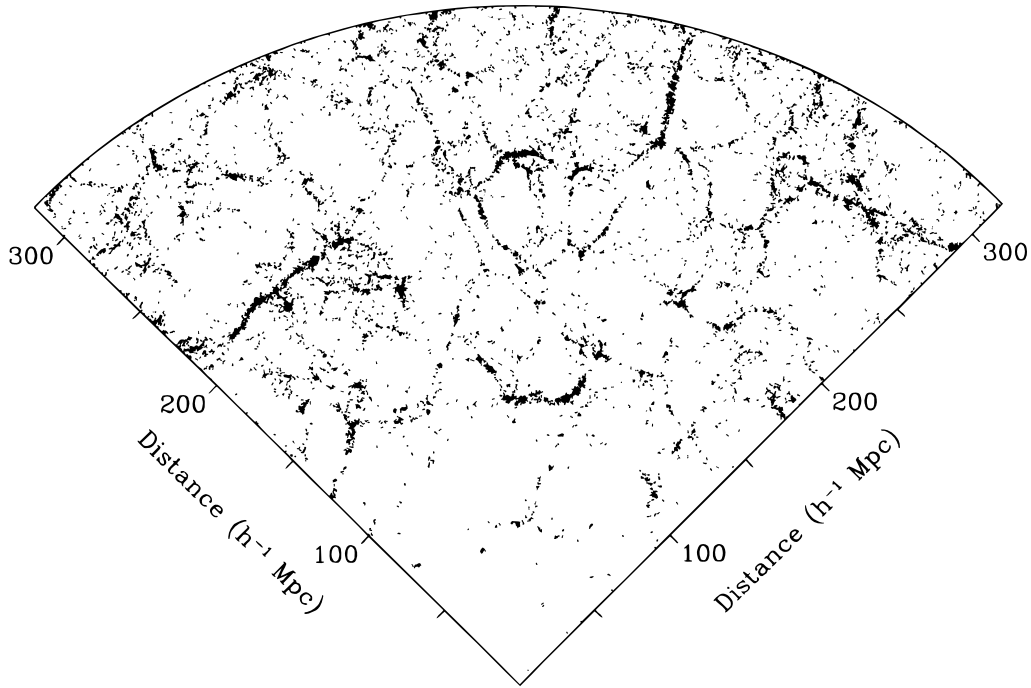
FIG. 5.—Slice of the simulation displaying the particle positions. The slice is $1°.5$ thick.

chosen luminosity function. This measured Ω may then be compared to the true value in the simulation, $\Omega = 0.4$.

Filament A has 296 galaxies at a distance of 22,000 km s^{-1}. We measure a velocity dispersion $\sigma_\perp = 400$ km s^{-1} and a length of 110 h^{-1} Mpc. This yields a mass of 7.9×10^{15} h^{-1} $M_\odot$ and $\Omega = 0.65$. Filament B has 305 galaxies at a distance of 14,000 km s^{-1}. We measure $\sigma_\perp = 450$ km s^{-1} and a length of 40 h^{-1} Mpc, yielding a mass of 3.6×10^{15} h^{-1} $M_\odot$ and $\Omega = 0.58$.

These two cases therefore yield overestimates of Ω by about 50%. The agreement between the estimated mass and the true mass is surprisingly good, bearing in mind the somewhat ambiguous choice of the member galaxies of the filament. In fact, by restricting ourselves to a $1°.5$ slice, we may have clipped out some galaxies that would have been included in the filament in a less two-dimensional survey; such galaxies lie just above or below the slice. Because the "fingers of God" are preferentially in the slice rather than
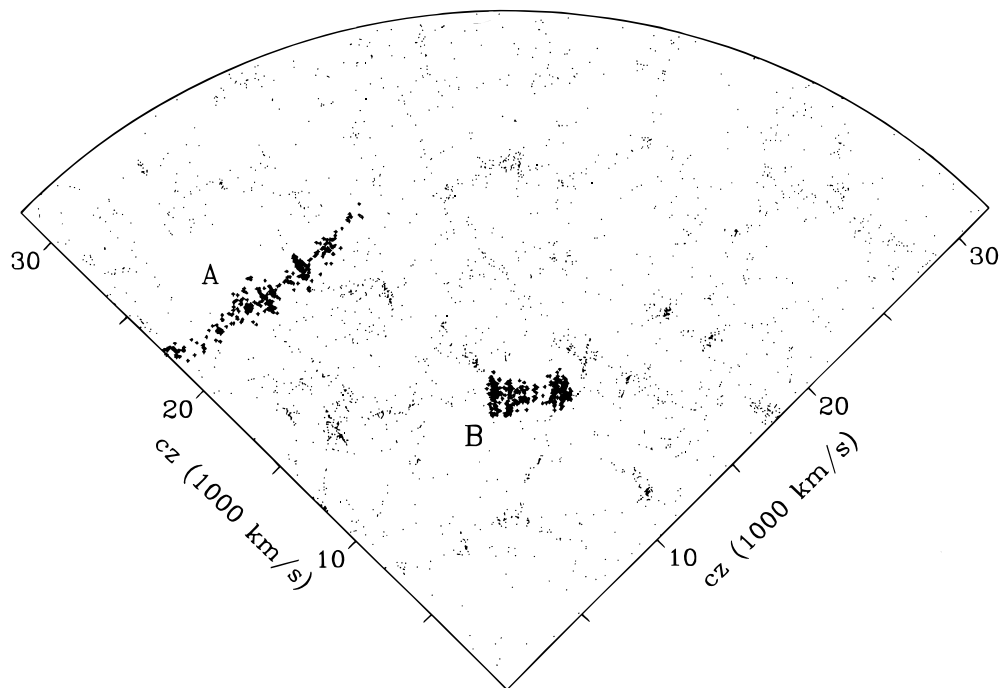

FIG. 6.—Mock redshift survey drawn from the slice displayed in Fig. 5. The two filaments analyzed in the text are marked with the letters A and B.

above or below, these additional galaxies would most likely not increase the velocity dispersion but would increase the "light" associated with the filament, thereby reducing the estimated value of Ω. This problem, combined with the difficulties in rejecting sheets, suggests that thin slices like the LCRS are less appropriate for this method than surveys with wider sky coverage such as the Sloan Digital Sky Survey (SDSS) (Gunn & Knapp 1993). The two cases presented here are merely intended to be illustrative; we discuss what is required for a full calibration and testing of the method in the next section.

4. DISCUSSION AND CONCLUSION

Motivated by the observation that the mass per unit length of an isothermal filament depends only on its velocity dispersion and not on its scale radius, we have proposed a method to measure the dynamical mass of large-scale filaments in galaxy redshift surveys. A filament aligned across the plane of the sky would have its velocity dispersion easily observable as the thickness of the filament in redshift space. The degree of substructure along the filament is also observable and might be used to warn against filaments that drastically violate the validity regime of our method. In a wide-angle redshift survey, such as CfA/SSRS (Vogeley et al. 1994; da Costa et al. 1994), 2-degree Field (Taylor 1995), or SDSS (Gunn & Knapp 1993), it should be possible to distinguish between one-dimensional filaments and two-dimensional sheets. The method could then be used to estimate the masses and mass-to-light ratios of these structures, which are up to 10 times more massive than rich clusters, and thus yield information on the behavior of the dark matter on these scales.

The bulk of the tests we present are performed on filaments selected from cross-sectional real-space slices of an $\Omega = 0.4$ simulation. We pick the radius of the filament to be the turnaround radius, here found as the radius at which the enclosed density is 5.7 times the background density. We find that the velocity dispersion of those particles, as measured from a direction perpendicular to the axis of the filament, is a good predictor of the mass contained within that radius. The ensemble of 23 filaments so treated yields an estimate that is biased $\sim 20\%$ high with a scatter $\sim 33\%$ (1σ).

However, a full test of the robustness of the method must be done in redshift space and not in real space. To illustrate the situation in redshift space, we have analyzed two case studies (see Figs. 5 and 6). However, we leave to a future paper the larger task of designing an automated Monte Carlo scheme to calibrate the method and prove its robustness. Such a program would begin from a cosmological simulation and extract a mock redshift survey. One would then apply a quantitative algorithm to this survey in order to identify filamentary structures and select member galaxies. With these filaments in hand, one would compute the velocity dispersion and convert it to a mass-to-light ratio or Ω. By considering many systems, one may tune and calibrate the selection method and determine the error in its estimates, possibly as a function of some substructure criteria. One could then repeat this using different cosmological simulations in order to show that the calibration is indeed robust against variations in the cosmological model.

Because the steady state assumption used in the derivation of equation (13) does not hold in cosmological situations, the coefficient of 2 in equation (13) is subject to

further calibration. Since the amount of infall depends upon the background cosmology, it is likely that a given calibration will not be unbiased in all cosmologies. In particular, the higher degree of present-day infall in $\Omega = 1$ models might cause systematic underestimates of the mass relative to a low Ω calibration. It will be important to quantify this effect so as to assess the method's ability to differentiate between cosmological models. Cylindrical self-similar solutions (Fillmore & Goldreich 1984) or secondary infall solutions (Gott 1975; Gunn 1977; Hoffman & Shaham 1985; Ryden & Gunn 1987) might provide analytic testbeds for understanding the relation between the virialized and infall regions and for probing the dependence of the results on the underlying cosmology.

The density-morphology relation of galaxies (Dressler 1980, 1984; Postman & Geller 1984) may produce a significant systematic effect on our mass estimate when combined with the selection criteria of an actual survey. Because elliptical galaxies prefer high-density regions and spirals conversely, a survey that favors one type over the other will weigh the regions of high- and low-velocity dispersion differently, thereby producing differing estimates of μ (see, e.g., differences between estimates of the bias factor in optical and *IRAS* surveys; Peacock & Dodds 1994). In extreme cases, the skewed selection function may affect the performance of the filament-finding algorithm. Similarly, a survey such as the LCRS, which undersamples close pairs, would affect the calculation of μ. Including a parameterized form of the density-morphology relation in the extraction of the mock surveys might allow one to treat the systematic differences between redshift surveys.

In this paper, we assumed that the galaxy distribution followed the mass distribution of the simulation and used simulation particles as galaxy tracers. Biased galaxy formation could significantly affect the validity of this treatment. Velocity bias (Carlberg & Couchman 1989; Couchman & Carlberg 1992; Carlberg 1994; Summers, Davis, & Evrard 1995) may cause the velocity of galaxies to be diminished relative to the dark matter, especially in denser regions. Estimates of this effect vary but are often $\sim 20\%$ for clusters; however, a comparison between optical and X-ray observations of clusters seems to indicate that the bias is less than a 10% effect (Lubin & Bahcall 1993). In addition, there is the possibility that some aspects of biasing are associated with the filamentary structure itself, e.g., if fragmentation of filaments affects galaxy formation. This would not be the case in a hierarchical structure formation model, in which the galaxy-scale perturbations should collapse well before the large-scale structure forms, leaving the galaxies to fall onto the filaments in a manner similar to the dark matter. Numerical work on velocity bias has focused on clusters, but could be extended to the filamentary case.

The Perseus-Pisces supercluster is the obvious nearby candidate to which our method can be applied, since its central ridge is a prominent linear structure stretching across the sky in redshift space (Haynes & Giovanelli 1986). To estimate the mass-to-light ratio, we use the data from the H I redshift survey of Giovanelli, Haynes, and collaborators (Wegner, Haynes, & Giovanelli 1993, and references therein). We focus on a restricted portion of the central ridge with (R.A., δ) corners of (0^h30^m, $27°$), (2^h15^m, $36°.5$), (2^h15^m, $40°.5$), and (0^h30^m, $31°$) in order to avoid the heavily extincted region near the Perseus cluster. We impose a heliocentric velocity cut of 4000 km s^{-1} < v < 5800 km

s^{-1}; the remaining 307 galaxies have a velocity dispersion (using 10 lengthwise bins to remove bulk motions) of 423 km s^{-1} and an average distance of 51 h^{-1} Mpc. Expanding the velocity cut by 600 km s^{-1} on both sides adds only 23 galaxies and increases the velocity dispersion to 490 km s^{-1}. The change in the mean velocity from one end of the region to the other is small (see Fig. 5 of Wegner et al. 1993), indicating that filament is very close to the plane of the sky and that the contamination of the velocity dispersion by motions along the filament should be negligible.

Using the first velocity cut, we infer a mass per unit length $\mu = 8.3 \times 10^{13}$ $M_{\odot}$ Mpc^{-1}, a length of 21 h^{-1} Mpc, and a mass $M = 1.7 \times 10^{15}$ h^{-1} $M_{\odot}$. Assuming that all of the selected galaxies are at a distance of 51 h^{-1} Mpc, imposing a uniform extinction correction of 0.2 mag (Giovanelli, Haynes, & Chincarini 1986), and assuming based on integrating the luminosity function (Marzke, Huchra, & Geller 1994) that the survey includes 56% of the light, we estimate the total B-band luminosity to be 3.9×10^{12} h^{-2} in solar units. Hence, we find $M/L_B \approx 450$ h in solar units; however,

the effects described earlier in this section, in particular the lack of a tested and calibrated redshift-space algorithm for determining which galaxies are members of the filament as well as the fact that this estimate is based on a single object, render this estimate uncertain within a factor of 2. Further refinements of the method and its application to additional filaments, as will be available with surveys such as the SDSS (Gunn & Knapp 1993), should substantially reduce these uncertainties.

REFERENCES

Baffa, C., Chincarini, G., Henry, R. B. C., & Manousoyanaki, J. 1993, A&A, 280, 20
Bahcall, N., Lubin, L., & Dorman, V. 1995, ApJ, 447, L81
Bertschinger, E., & Gelb, J. M. 1991, Comput. Phys., 5, 164
Binney, J., & Tremaine, S. 1987, Galactic Dynamics (Princeton: Princeton Univ. Press)
Bond, J. R., Kofman, L., & Pogosyan, D. 1995, astro-ph/9512141
Bond, J. R., & Myers, S. 1996, ApJS, 103, 1
Carlberg, R. G. 1994, ApJ, 433, 468
Carlberg, R. G., & Couchman, H. M. P. 1989, ApJ, 340, 47
Cen, R., & Ostriker, J. P. 1994, ApJ, 431, 451
Chandrasekhar, S., & Fermi, E. 1953, ApJ, 118, 115
Couchman, H. M. P., & Carlberg, R. G. 1992, ApJ, 289, 453
da Costa, L. N., et al. 1994, ApJ, 424, L1
David, L. P., Jones, C., & Forman, W. 1995, ApJ, 445, 578
de Lapparent, V., Geller, M. J., & Huchra, J. P. 1986, ApJ, 302, L1
Dressler, A. 1980, ApJ, 236, 351
———. 1984, ARA&A, 22, 185
Einasto, J., Joeveer, M., & Saar, E. 1980, MNRAS, 193, 353
Eisenstein, D. J., & Loeb, A. 1995, ApJ, 439, 520
Fillmore, J. A., & Goldreich, P. 1984, ApJ, 281, 1
Gehman, C., Adamas, F., Gatuzzo, M., & Watkins, R. 1996, ApJ, 457, 718
Geller, M. J., & Huchra, J. P. 1989, Science, 246, 897
Giovanelli, R., Haynes, M. P., & Chincarini, G. L. 1986, ApJ, 300, 77
Gott, J. R. 1975, ApJ, 201, 296
Gunn, J. E. 1977, ApJ, 218, 592
Gunn, J. E., & Knapp, J. 1993, ASP Conf. Ser. 43, Sky Surveys, ed. B. T. Soifer (San Francisco: ASP), 267
Haynes, M., & Giovanelli, R. 1986, ApJ, 306, L55
Hoffman, Y., & Shaham, J. 1985, ApJ, 297, 16
Inutsuka, S., & Miyama, S. 1992, ApJ, 388, 392
Jungman, G., Kamionkowski, M., Kosowsky, A., & Spergel, D. N. 1996, Phys. Rev. Lett., 76, 1007
Kaiser, N. 1987, MNRAS, 227, 1

Landy, S. D., Shectman, S. A., Lin, H., Kirshner, R. P., Oemler, A. A., & Tucker, D. 1996, ApJ, 456, L1
Larson, R. B. 1985, MNRAS, 214, 379
Lin, H., Kirshner, R. P., Shectman, S. A., Landy, S. D., Oemler, A., Tucker, D. L., & Schechter, P. L. 1996, ApJ, 464, 60
Lubin, L. M., & Bahcall, N. A. 1993, ApJ, 415, L17
Marzke, R. O., Huchra, J. P., & Geller, M. J. 1994, ApJ, 428, 43
Milgrom, M. 1997, ApJ, in press
Ostriker, J. 1964, ApJ, 140, 1056
Park, C., Vogeley, M., Geller, M., & Huchra, J. P. 1994, ApJ, 431, 569
Peacock, J. A., & Dodds, S. J. 1994, MNRAS, 267, 1020
Peebles, P. J. E. 1993, Principles of Physical Cosmology (Princeton: Princeton Univ. Press)
Postman, M., & Geller, M. J. 1984, ApJ, 281, 95
Postman, M., Geller, M. J., & Huchra, J. P. 1988, AJ, 95, 267
Press, W. H., Teukolsky, S. A., Vetterling, W. T., & Flannery, B. P. 1992, Numerical Recipes in C (second ed; Cambridge: Cambridge Univ. Press)
Raychaudbury, S., Fabian, A. C., Edge, A. C., Jones, C., & Forman, W. 1991, MNRAS, 248, 101
Rubin, V. C. 1983, Sci. Am., 248, 96
Ryden, B., & Gunn, J. 1987, ApJ, 318, 15
Sargent, W. L. W., & Turner, E. L. 1977, ApJ, 212, L3
Shectman, S. A., Landy, S. D., Oemler, A., Tucker, D. L., Lin, H., Kirshner, R. P., & Schechter, P. L. 1996, ApJ, 470, 172
Stodółkiewicz, J. S. 1963, Acta Astron., 13, 30
Strauss, M., & Willick, J. 1995, Phys. Rep., 261, 271
Summers, F. J., Davis, M., & Evrard, A. E. 1995, ApJ, 454, 1
Taylor, K. 1995, BAAS, 186
Trimble, V. 1987, ARA&A, 25, 423
Vogeley, M. S., Park, C., Geller, M. J., Huchra, J. P., & Gott, J. R. 1994, ApJ, 420, 525
Wegner, G., Haynes, M. P., & Giovanelli, R. 1993, AJ, 105, 1251
Zel'dovich, Ya.B. 1970, A&A, 5, 84